

CHARACTERIZATION OF CRYOGENIC SPRAY NOZZLES WITH APPLICATION TO SKIN COOLING

Guillermo Aguilar^{1,*}, Boris Majaron^{2,4}, Wim Verkruyse², J. Stuart Nelson², and Enrique J. Lavernia³

¹Whitaker Center for Biomedical Engineering
University of California, Irvine
Irvine, CA 92697

²Beckman Laser Institute and Medical Clinic
University of California, Irvine
Irvine, CA 92612

³Department of Chemical and Biochemical Engineering and Materials Sciences
University of California, Irvine
Irvine, CA 92697

⁴Jozef Stefan Institute
Jamova 39, SI-1000 Ljubljana
Slovenia

ABSTRACT

Cryogenic sprays are used for cooling of human skin during laser treatments of hypervascular lesions, such as Port Wine Stain birthmarks. In this work, six straight-tube nozzles, including two commercial nozzles, are characterized by obtaining photographs of cryogenic spray shapes, as well as measurements of the average droplet diameter, velocity and temperature. An evaporation model is used to predict the evolutions of average droplet diameter and temperature. The results show two distinct spray patterns—jet-like sprays for *wide nozzle* diameters, and cone-like sprays for *narrow nozzle* diameters. The *wide nozzles* show significantly larger droplet diameters, larger velocities and higher temperatures, as all these variables are measured as a function of distance from the nozzle. These results complement and support previously reported results, where it was shown that *wide nozzles* are capable of producing larger heat transfer coefficients than those obtained with *narrow nozzles*.

T average temperature [$^{\circ}\text{C}$ or K]
 V bulk or average velocity [m/s]
 z distance from the nozzle [mm]

Greek

ρ density [Kg/m^3]
 λ' evaporation constant [m^2/s]

Subscripts

a air
 d relative to the droplet
 g relative to the air-cryogen vapor mixture
 l liquid
 s relative to the surface
 ∞ relative to ambient
 0 initial
 1 relative to time t_1

NOMENCLATURE

c specific heat at constant pressure [J/kg K]
 D droplet diameter [μm]
 k thermal conductivity [W/m K]
 L latent heat of vaporization [J/kg]
 m mass [mg]
 Nu Nusselt number
 Pr Prandtl number
 Re Reynolds number

1. INTRODUCTION

The use of sprays and other physical dispersions of droplets or small particles is important for many processes and engineering applications, such as in agricultural chemicals, application of paints, drying of wet solids, cooling of nuclear cores, dispersing liquid fuels for combustion, etc. Despite the fact that several studies have been carried out on liquid sprays [1-3], as well as on liquid fuel sprays [4,5], limited information exists on the thermodynamics of cryogenic

* Corresponding author: Beckman Laser Institute and Medical Clinic,
University of California Irvine, Irvine, CA 92612. e-mail: gaguilar@bli.uci.edu

sprays. Pioneering work on this subject was carried out by Ingebo [6-8], who offered useful correlations that predict mean particle size diameters of cryogen sprays produced by two-fluid nozzles, based on gas mass flux, cryogen and gas properties. Estes and Mudawar [9] studied the evaporation efficiency of water and Fluorinert™ (Fluorocarbon compounds) sprays by measuring heat flux across a sprayed surface and its variation with surface temperature and flow rate.

With respect to the use of cryogenic sprays for laser treatment of port wine stain birthmarks (PWS)—which is the application of interest of this work, a few papers summarize the work developed until now [10-16]. To remove these birthmarks, patients are treated with laser pulses that induce permanent thermal damage to the PWS blood vessels, typically located 200 to 550 μm below the skin surface (within the dermis) [13]. However, since the absorption of laser energy by melanin localized within the superficial skin layer (epidermis) can cause undesirable epidermal damage, such as scarring or dyspigmentation [14], short spurts of cryogen are sprayed on the skin prior to the laser pulse [15], so the epidermis remains protected. In order to achieve optimal cooling of the epidermis with minimal cooling of the target PWS blood vessels (cooling selectivity), it is necessary to precisely control the precooling time [16]. This control favors cryogen spray cooling (CSC) over alternative approaches for skin cooling [12].

Although PWS laser therapy has been available for several years, more work is required to better understand the spray characteristics produced by different nozzles, as well as identify how these can be modified for optimum cooling selectivity.

The evaporation process of cryogenic sprays dictates, in part, how efficiently a particular spray is capable of removing heat from the skin surface, and thus requires particular attention. Evaporation in the discussed application should be understood in the context of two distinct processes. The first, taking place during *spray droplets travel* from the nozzle to the target, is related to the portion of the atomized liquid, which evaporates and extracts latent heat from the remaining liquid droplets. This causes overall cooling of the spray, often below the boiling temperature of the cryogen. The other process is the evaporation of the cryogen *at the skin surface*, which determines primarily the efficiency of heat extraction from the skin. Both processes need to be studied in conjunction for the appropriate implementation of CSC in dermatology.

In this work, the *spray droplets travel* and the related evaporation processes are studied via droplet flight profile characterization. In particular, the focus is on the characterization of atomizing nozzles of different geometries, based on spray shape imaging, evolution of average droplet diameter D , average velocity V , and average temperature T . First, the effect of nozzle diameter (D_N) and length (L_N) on the general spray characteristics is studied. For that purpose, four straight-tube nozzles of different lengths and diameters were built. With the aid of fast flash lamp photography (FFLP) we observe the spray shapes produced by these four nozzles and two commercial nozzles (ScleroPLUS™ and GentleLASE™ by Candela, Wayland MA), as well as the formation of frost at the sprayed areas. Also, with the aid of an ensemble particle concentration and sizing device (EPCS), time-of-flight procedure (TFP), and a miniature thermocouple sensor, the evolution of D , V , and T as functions of distance from the nozzle tip, z , are measured. From these trends, values at the exit of the nozzles, *i.e.*, D_0 , V_0 , and T_0 are estimated. Using these estimates, in combination with a single-droplet evaporation model, T can be predicted as a function of z , *i.e.*, $T(z)$, as discussed by Aguilar *et al.* [17,18]. Finally, these results are discussed in the context of those

obtained during recent studies on the cryogen evaporation *at the skin*, and its effects on skin temperature evolution [19,20].

2. EXPERIMENTAL SETUPS AND PROCEDURES

2.1 Spray Forming Setup

Four straight-tube nozzles were constructed at the Beckman Laser Institute (BLI), University of California at Irvine (UCI). Their geometry resembles that of two commercial nozzles used for PWS and hair removal laser treatments, *i.e.*, ScleroPLUS™ and GentleLASE™ (Candela, Wayland, MA), respectively, which were also used in this study. The four custom-made nozzles were made of stainless steel tubes of two different lengths (L_N) and two different inner diameters (D_N), and a copper body fitted tightly around an auto fuel injector used to control the spurt duration electronically. From available dimensions of L_N and D_N , a short wide (SW), long wide (LW), short narrow (SN) and long narrow (LN) nozzles were constructed. Table 1 shows dimensions of these four nozzles as well as those developed by Candela.

The cryogen is always delivered through a standard high-pressure hose connecting the cryogen vessel to the fuel injector. This vessel is a commercial HFC-134a cryogen container, which is pressurized at the saturation pressure of this cryogen at room temperature (6.7 bar at 25°C).

2.2 Imaging Setup

A progressive-scan CCD camera with shutter speed of 60 μs (9700 TMC by Pulnix, Sunnyvale, CA) is used to take photographs of the spray shapes, and the frost formed on the sprayed target after the spurts end. A flash lamp (FX-1160 by EG&G Electronics, Salem, MA) provides illumination gating by about 5 μs long pulses that “freeze” the image of flying cryogen droplets. The supporting electronics enable acquisition of image sequences at 30 frames per second, with precisely controlled delays with respect to the onset of the cryogen spurt. The flashlamp and the camera are positioned in the same horizontal plane, with the camera viewing perpendicularly to the spray axis and all images are taken under equal lighting conditions. To obtain spray shape images, the camera is placed 130 mm away from the nozzle tip, and the flashlamp directed towards the nozzle tip at a 30° angle with respect to the camera axis. With this arrangement it is possible to obtain a field of view of about 17 \times 14 mm.

For the photographs of the cryogen sprayed target, a rectangular epoxy block is used. The camera is positioned perpendicular to the spray block, at a distance of about 130 mm, and the flashlamp placed at about 80 mm away from the block surface, at a 45° angle from the camera. The spray is aimed to the block from the opposite side of the flash at an angle of approximately 20° with respect to the normal to the block.

2.3 Droplet Size Measurements

An Ensemble Particle Concentration & Sizing apparatus (EPCS by Insitec/Malvern, Worcestershire, UK) is used to measure average diameters (D) of the spray droplets. This instrument is based on the principle of diffraction of a parallel beam of monochromatic light (provided by a 670 nm diode laser) caused by the spray droplets. When this beam is obstructed by spray droplets, a diffraction pattern is formed. If the spray is monodisperse, the diffraction pattern is made of a series of alternate light and dark concentric rings (Fraunhofer diffraction), and the spacing between these rings is related to the

droplet diameter. For polydisperse sprays, a number of these Fraunhofer patterns are superimposed, but the overlapping diffraction rings may still be associated with a characteristic droplet diameter size range. A more detailed description may be found in Lefevbre [21]. In order to obtain more localized measurements of D , the beam is reduced from its normal diameter of 10 mm to about 3.3 mm with the aid of an inverted beam expander (OptoSigma, Santa Ana, CA). A positioning system is used to displace the nozzles tip perpendicularly to the laser beam, from about 15 to 200 mm.

As a meaningful measurement of particle size, the Sauter mean diameter (SMD or D_{32}) is utilized and represents the size of a droplet with the same surface area to volume ratio as that of the entire spray. This mean droplet diameter is known to characterize heat and mass transfer of the spray better than the arithmetic mean of the droplet diameter [21].

2.4 Droplet Velocity and Spray Development Time

In order to estimate the droplet velocity (V), we developed an experimental procedure, which we refer to as time-of-flight procedure (TFP). This procedure utilizes a continuous laser beam (He-Ne laser, 633nm) aimed at a fast photo detector. The output signal of the photo detector is recorded by a digital oscilloscope (TDS3054 Tektronix, Beaverton OR). The nozzle is positioned at a known distance, z , perpendicular to the laser beam, so that when the spray droplets are ejected from the nozzle, the beam is obstructed and the signal intensity decreases. By conducting measurements at two distances (z_1 and z_2), it is possible to determine the difference in time between the first signs of attenuation of both signals (Δt), and thus, compute V for different positions along the spray axis (i.e., $V = (z_2 - z_1) / \Delta t$). Figure 1a shows a sketch of this experimental procedure along with an example (Fig. 1b) of the data recorded using the LW nozzle, with the tip positioned at 123 and 153 mm away from the laser beam, respectively. It is important to notice that V is the average velocity with respect to distance, but it represents the velocity of the fastest moving droplets.

Besides estimating V , this procedure also determines the spray development time (t_d), i.e., the time it takes for the spray to reach a stable steady state condition. To do this, one should look at the difference in time between the point where the signal starts to diminish and that where the signal starts to oscillate around a mean value (Fig. 1c).

2.5 Droplet Temperature Measurements

A type-K thermocouple with bead diameter of approximately 0.3 mm (5SC-TT-E-36 by Omega, Stamford, CT) is used to measure the average spray temperature as a function of distance from the nozzle tip, $T(z)$. The estimated response time for this thermocouple is about 40 ms in still water at 100°C, and its ASTM standard wire error is below $\pm 2.2^\circ\text{C}$ for the range of temperatures measured. Cryogen spurt durations of at least 1 second are used, which ensure steady state conditions for the thermocouple. The temperature sensor is supported by a rigid stick and inserted into the center of the spray cone at varying distances from the nozzle. The estimated uncertainty in z is ± 0.5 mm. Since water condensation and freezing on the thermocouple bead could affect temperature measurements, these experiments are conducted in a chamber filled with dry air (relative humidity below 5%). Under such conditions, most of the tests do not show appreciable condensation, except for $z > 100$ mm, where signs of frost formation are observed on the thermocouple bead.

3. THEORETICAL EVAPORATION MODEL

In a recently conducted work [17,18], a single-droplet model is used to estimate the average diameter (D), velocity (V), temperature (T), and evaporation rate ($\delta m' / \delta t$) of the entire cryogenic spray. This model describes the evolution of D , V , T and $\delta m' / \delta t$ with time, and in summary, it is given by the following four Equations:

$$D^2 = D_0^2 - \lambda' t, \quad (1)$$

where D_0 is the initial droplet diameter, and λ' is the evaporation constant under forced convection conditions,

$$V = V_0 - \left(\frac{F_D t}{m_0 - \frac{\delta m'}{\delta t} t} \right), \quad (2)$$

where V_0 is the initial droplet velocity, F_D the drag force causing deceleration of a round sphere of surface area A , and m_0 is the initial mass of a single droplet,

$$T_1 = \frac{m_0 c_l T_o - (m_0 - m_{1,l})L + \int Nu k_g \pi D [T_\infty - T(t)] dt}{m_{1,l} c_l + (m_0 - m_{1,l}) c_g}, \quad (3)$$

where m , c , L , Nu and k stand for the instantaneous droplet mass, specific heat at constant pressure, latent heat of vaporization, Nusselt number and cryogen thermal conductivity; and the subindices 0, 1, l and g stand for initial, arbitrary time 1, liquid cryogen and gas cryogen, respectively. By successive iterations, Eq. (3) allows one to estimate the average droplet temperature at time t_1 , from initial values D_0 , V_0 , and T_0 . In order to obtain $T(z)$, the distance that a single droplet travels in time t_1 is computed by integrating Eq. (2) over time, i.e., $z =$

$$\int_0^{t_1} V dt.$$

Finally, the evaporation rate can be computed by:

$$\frac{\delta m'}{\delta t} = 2\pi D \left(\frac{k_g}{c_g} \right) \ln(1 + B_M) [1 + 0.3 Re_d^{0.5} Pr_g^{0.33}] \quad (4)$$

where Re_d and Pr_g are the droplet Reynolds and Prandtl numbers, and B_M is the mass transfer number. The term in square brackets in Eq. (4) accounts for forced convection due to relative motion of the droplet with respect to surrounding air.

In this work, the TFP is used to get better estimates of both V_0 and V , rather than computing them based on the assumption of single-phase turbulent flow within the nozzle and Eq. 2, respectively, as it was done previously [17,18]. The reason for this is that the effect of the drag force on V as represented by Eq. 2 appeared to be negligible in the previous studies, although experimental data presented herein suggest a more important contribution.

4. RESULTS

Figure 2 shows photographs of the spray shapes produced by the four straight-tube nozzles and two Candela nozzles: ScleroPLUS™ and GentleLASE™. For the two *wide nozzles*, SW and LW (Figs. 2a and 2b), the cryogen exits the nozzle in a jet-like fashion, while with the *narrow ones*, SN and LN (Figs. 2c and 2d), a cone-shaped spray is

appreciable. The higher intensity of the reflected light, indicates that with the *narrow nozzles*, the cryogen is more finely atomized than with the *wide* ones. Although the effect of nozzle length in the spray characteristics seems to be less pronounced than the effect of diameter, a somewhat finer atomization is appreciable for the short nozzles than for the long ones. Photographs of the Candela nozzles (Figs. 2e and 2f) appear to show very different characteristics between them. However, it should be mentioned that using the dynamic cooling device (DCDTM) and handpieces provided by the manufacturer, the ScleroPLUSTM handpiece housing obstructs the view of the spray outlet and causes some droplet scatter appreciable in Fig. 2e. The GentleLASETM, in contrast, shows a well-defined cone shape spray, similar to that of the *narrow nozzles*. Leaving this design problem aside, both Candela nozzles seem to cause similar degrees of atomization as the *narrow nozzles*. Therefore, based on these photographs, it appears reasonable to distinguish between those sprays with fine atomization (Candelas' and *narrow nozzles*) and others with somewhat coarser atomization (*wide nozzles*).

Figure 3 shows SMD measurements carried out with the EPCS/Insitec for the four straight-tube and the two Candela nozzles. Squares illustrate results for the *wide nozzles*, circles those obtained for the *narrow nozzles*, and the triangles the Candela ones. Error bars representing the estimated standard deviations are included on each data point. The first characteristic to point out is that there is practically no variation in D between the *wide nozzles*, nor between the Candela and *narrow nozzles* within the range covered. These measurements confirm the existence of the two atomization patterns pointed out above. A pattern of smaller droplet diameters, varying between 2 and 5 μm , produced by the Candela and the *narrow nozzles*, and another pattern with somewhat larger droplet diameters (between 12 and 15 μm), produced by the *wide nozzles*. Also shown in Fig. 3, are the evolutions of the droplet diameters based on Eq. 1. The initial droplet diameter (D_0) is a free parameter that needs to be adjusted. For these experimental data, values of D_0 of 25 μm and 14 μm for the *wide* and *narrow nozzles*, respectively, are the most appropriate to represent the variation of D with z within the range of 90 to 200 mm. The initial and instantaneous velocities, V and V_0 , which are also required in the model, are estimated from TFP experiments, presented next.

Figure 4 shows results of TFP experiments performed with the four straight-tube nozzles, in the manner described in Section 2.4. For each nozzle, measurements were carried out at five different distances from the nozzle tip (z), namely, 3, 63, 93, 123, and 153 mm. At each location, a total 8 spurts were averaged to obtain an average value of the signal. The computed velocities represented by the symbols in Fig. 4 are plotted against the mid distance between the 3 to 33, 33 to 63, and 123 to 153 mm ranges, *i.e.*, 15, 45 and 135 mm. As indicated by the error bars, the uncertainty of these measurements is somewhat large since the values depend on the choice of the point where the signal starts to decrease, and variation can be as great as ± 5 m/s. For this reason, a linear regression is sufficient to illustrate the evolution of the average droplet velocity with distance. The extrapolation of this regression to $z = 0$ is used to determine V_0 for each of the nozzles, which are rounded to 80, 60, 30 and 15 m/s for the SW, LW, SN and LN nozzles, respectively. As mentioned earlier, the TFP also allows one to determine the spray development time (t_d), which appears to be in the order of 25 ms, as shown in Fig. 1.

Figure 5 shows droplet temperature measurements as a function of z using a bare thermocouple. Squares represent the measurements obtained for the *wide nozzles*, and circles those carried out for the *narrow nozzles*. Also, the temperature measurements carried out for both Candela nozzles are shown with triangles for comparison. As the

photographs and droplet diameter measurements suggest, both Candela nozzles show a similar temperature evolution to those of the *narrow nozzles*. The lines represent computations of $T(z)$ resulting from Eq. (3) for all straight-tube nozzles. T_0 is also a free parameter, which needs to be either measured or estimated in the model. In all cases, it is very difficult to obtain a reliable measurement of $T(z)$ for $z < 1.5$ mm. At such short distances from the nozzle exit, the temperature fluctuates by about 5°C (as indicated by the error bars in that region). In this case, T_0 is adjusted until $T(z)$ matches the experimental data best, which for the *wide nozzles* is true for $T_0 = -26$ °C, and for the *narrow nozzles* true for $T_0 = -29$ °C. For *wide nozzles*, predicted curves reproduce the experimental data reasonably well up to about $z = 100$ mm. For $z > 100$ mm, the model predicts somewhat lower temperatures. For *narrow nozzles*, predictions cover the distances to about 90 or 120 mm, which is also coincident with the values at which a sudden temperature raise is measured, reflecting complete droplet evaporation.

In another set of experiments using the FFLP setup, cryogenic spurts were aimed at an epoxy block in the manner described in the Section 2.2. Figure 6 shows the frost that forms around the sprayed area, two seconds after the end of 50 ms spurts from (a) ScleroPLUSTM, (b) SN and (c) SW nozzles, respectively. In all cases, there is a bright region denoting the frost ring, which slowly diminishes in size with time. However, for the ScleroPLUSTM nozzle, the amount of frost surrounding the center of the spray after two seconds, is significantly larger than that for the SN; and in turn, the frost of the SN nozzle somewhat larger than that of the SW nozzle. These images illustrate the problematic issue of frost formation, seen during clinical treatments with the current commercial nozzle designs, and the possible benefit in reducing this frost simply by modifying nozzle geometry.

5. DISCUSSION

Based on photographs of spray shapes (Fig. 2), it is apparent that the variation of the nozzle length (L_N) does not have a significant impact on the overall characteristics of sprays produced by the straight-tube nozzles. This qualitative observation is also confirmed by the diameter measurements (D) shown in Fig. 3, and by spray temperature measurements (T) shown in Fig. 5, which show negligible differences between sprays produced by the *narrow nozzles*, on one hand, and those by the *wide nozzles*, on the other. Also, the Candela nozzles resemble the *narrow nozzles* in terms of their $D(z)$ and $T(z)$.

It is noticed in Fig. 3 that it was not possible to obtain reliable diameter measurements closer than 90 mm from the nozzle tip for the *wide nozzles*, most likely because of a too high density of spray, or even an unbroken jet (Figs. 2a,b). In contrast, for the *narrow nozzles*, it is possible to resolve the diameter measurements down to 15 mm since the sprays are better atomized (Figs. 2c,d). The GentleLASETM and ScleroPLUSTM spray droplets show similar diameter and trend than those of the *narrow nozzles*, in accordance with the spray similarities suggested from the photographs shown in Fig. 2. It was speculated in our previous work that the experiments with *wide nozzles* suggested a slight increase in D , or at least a tendency for it to remain invariant within the range of z from 90 to 150 mm. This behavior suggests the possibility of droplet coalescence, a phenomenon observed earlier in liquid and metal spray studies [22,23]. Indeed, droplet coalescence may occur if there is particle reentrainment and development of recirculation zones, as reported in earlier spray studies [24,25]. This observation is supported by this study, where the D measurements of SN and LN nozzle sprays show more clearly a maximum between 60 and 70 mm. Interestingly, the

ratio between the *narrow nozzles* and the GentleLASE™ diameters is 1.8, and no significant difference is appreciable in terms of their spray shapes, droplet diameter and temperature evolutions. On the other hand, the ratio between the *narrow* and *wide nozzles* diameters is slightly larger (2.0), and yet the difference in terms of their spray shapes, diameter and temperature evolutions is noteworthy. This large change in spray characteristics for a relatively similar nozzle diameter ratio indicates that there is a critical nozzle diameter—somewhere between 31.8 and 63.5 mm, at which a change in the atomization mechanism takes place (at least, for the particular conditions under which this cryogen is sprayed).

Even though the evolution of the droplet diameter predicted by the model is very similar for both the *wide nozzles* and the *narrow nozzles*, a slight effect of the nozzle length is appreciable in each case, where the short nozzles systematically show smaller D at the same z . The reason for this variation is presumably related to different droplet velocities corresponding to each nozzle, as seen in Fig. 4. Since the cryogen vessel pressure is the same for all nozzles, V_0 and V differ between nozzles because the different diameters and lengths impose different levels of drag to the flowing cryogen. Longer nozzles with smaller diameter impose the largest drag, and thus, the lowest velocities; while shorter nozzles with larger diameters have the lowest drag, and thus, the highest velocities. In particular, for a given nozzle diameter, the short nozzles have lower drag, which then produces higher velocities than longer nozzles at the same z (Fig. 4). Since the evaporation rate is higher for a faster moving particle droplet, this produces, on average, smaller droplet diameters for the shorter nozzles (Fig. 3). It should be noted that the predictions of the model for the diameter evolutions of the *narrow* and Candela nozzles are not as good as those for the *wide nozzles*. This is simply an indication that the D^2 -law model used to describe the diameter evolutions is too crude of an approximation. More detailed work is currently conducted to address this issue.

In our previous work [17,18], preliminary values for V_0 were estimated based on the assumptions of a fully developed-single phase flow within the nozzle, and considering that pressure drops along the hose and across the solenoid valve were negligible. Furthermore, the instantaneous droplet velocity (V) was computed assuming a drag force acting around the droplet surface (Eq. 2). However, it was later observed that droplet deceleration predicted by this Equation was not causing a significant velocity decrease, as the experimental data of this work show. Therefore, in this work, the instantaneous velocity (V) is computed from a linear regression through TFP data, and the initial velocity parameter (V_0) is obtained by the intercept of this linear regression. Although this approach is presumably more accurate, it is likely that TFP overestimates the instantaneous velocity (V), because it measures essentially the velocity of the fastest moving droplets.

The variation of temperature with distance for all nozzles shown in Fig. 5 is consistent with the expected results. For those sprays that are more finely atomized, *i.e.*, have a larger surface area, removal of latent heat of vaporization from the remaining liquid droplets is more effective, and thus lower temperatures are achieved. Notice that the initial temperature T_0 , does not seem to be the same for the *narrow* and *wide nozzles*. For the *wide nozzles*, T_0 is equal to -26°C , which coincides with the boiling temperature of the cryogen ($T_b = -26^\circ\text{C}$), and it is the expected cryogen temperature after a sudden expansion through the valve (provided the evaporation within the hose is negligible). This means that the cryogen has not been significantly atomized, and thus, that the liquid cryogen has not been able to undercool. On the other hand, the T_0 estimated for the *narrow nozzles* is equal to -29°C , which indicates better atomization right at the exit of

the nozzle (and perhaps even some degree of evaporation within the nozzle), and thus, a larger undercooling. This interpretation is also consistent with photographs shown in Fig. 2, where the *narrow nozzles* show better atomization than the *wide nozzles* close to the nozzles exit. Even though this speculation seems plausible, it should be emphasized that T_0 , as well as D_0 and V_0 , are model parameters that need to be adjusted somewhat arbitrarily, and thus, their absolute values may not represent the physical reality.

It is also worthwhile mentioning that the proposed evaporation model, which was only tested with *wide nozzles* in our previous study [18], predicts quite accurately the temperature evolution of *narrow* ones as well. As in our previous study, T_0 has been adjusted to fit best the range of $10 < z < 100$ mm, rather than the range of $z > 100$ mm. The reason being that despite provisions taken to eliminate most of the moisture from air during these experiments, some signs of condensation and frost formation on the thermocouple were noticed, in particular for $z \geq 150$ mm. In fact, the experimental temperature measurements show higher values than those predicted by the model at such distances. This is likely due to release of latent heat of water vapor on the thermocouple, which is not considered by the model.

As reported by Svaasand *et al.* [20], there is a significant difference in the values of the interface heat transfer coefficient (h_{cryo}) between the two distinctive spray patterns discussed in this work. Values between 6000 to $8500 \text{ Wm}^{-2}\text{K}^{-1}$ are reported for the SN nozzle, and values of about $10800 \text{ Wm}^{-2}\text{K}^{-1}$ for the SW nozzle. Verkruyssen *et al.* [19] attributed similar differences to the build up of a cryogen layer on the sprayed surface, which appears to be thicker in the case of the SN nozzle as compared with the SW nozzle, and thus constitutes a higher thermal barrier for heat extraction. This hypothesis is supported, in part, by the longer lasting frost seen for the SN in comparison with the SW nozzle (Fig. 6). Also, it was speculated [19] that the different cryogen layer thickness was due to the larger momentum (basically given by the product of D and V) of large and fast moving droplets, such as those produced by *wide nozzles*, in contrast to the smaller and slower moving droplets produced by *narrow nozzles*. Droplets with higher momentum are capable of piercing through, and even removing the cryogen layer on the surface, evaporate on the skin surface, and consequently, remove heat more efficiently. By way of contrast, droplets with lower momentum do not penetrate the cryogen layer, and thus, they allow the formation of a thick layer with consequent build up of a thermal barrier, which diminishes efficiency of heat extraction.

In an ideal situation of evaporative heat extraction, cryogen droplets adhere to the skin surface, lose all radial momentum as quickly as possible, and subsequently evaporate. According to the present studies, this situation may only be possible if the atomization process is such that a liquid stream of sufficient large size and high velocity droplets is provided, or alternatively, if smaller and lower velocity droplets are deposited on the skin, but at a lower flow rate, so no thick cryogen layer is built. A byproduct of the latter solution would be the reduction of the frost formation at the sprayed area (Fig.6).

In relation to the commercial devices, it is also reasonable to say that these studies show that it may be possible to increase the heat transfer coefficient that their sprays produce, simply by replacing the current nozzles with larger diameter ones, although this may not be strictly necessary for PWS treatments [20]. One should be aware, however, that a variation in the nozzle diameter could cause a variation of the sprayed area—as evidenced by the jet-like and cone-like sprays (Fig.2), which may also pose some practical complications.

6. CONCLUSIONS

1. Two distinctive spray patterns of cryogenic spray shapes have been identified for the six nozzles used in this study. The first pattern—jet-like sprays, produced by the *wide nozzles* with ID of 1.4 mm; and the second pattern—cone-like sprays, produced by the Candela and *narrow nozzles* with ID ranging from 0.51 to 0.76 mm. The nozzle length (L_N) does not seem to have a large impact on the spray characteristics;
2. Each of these two spray patterns shows distinctive evolutions of average droplet size D , velocity V , and temperature T . The Candela and *narrow nozzle* sprays show average droplet diameters ranging between 2 and 6 μm , exit velocities (V_0) for the *narrow nozzle* sprays vary between 15 and 30 m/s, and temperatures vary between -29 and -57°C , for the range of distances z covered (0 to 250 mm). The *wide nozzle* sprays show average droplet diameters ranging between 12 to 15 μm , exit velocities vary between 60 and 80 m/s, and temperatures varying between -26 to -60°C for the same range of distances studied;
3. The proposed evaporation model represents the evolution of T reasonably well, provided the free parameters D_0 , V_0 and T_0 are properly selected. However, prediction of D is not as good for Candela and *narrow nozzles*, as it is for the *wider* ones, indicating that use of the D^2 -law model to predict the diameter evolution, may simply be a very crude approximation; and
4. A very strong relationship is established where basically two different kinds of spray patterns can be related to two heat extraction processes. These results indicate that the h_{cryo} produced by the *narrow nozzles*, and presumably by the Candela nozzles as well, can still be increased, provided that a larger nozzle diameter is substituted.

ACKNOWLEDGMENTS

The authors wish to acknowledge the financial support from the Whitaker Foundation, the equipment donation and Grant (No. 482560-59109 to E.J.L and J.S.N), as well as useful feedback from Karl Pope and Jim Hsia, of Candela Corp. We also acknowledge the support from the Institute of Arthritis and Musculoskeletal and Skin Diseases, research grant awarded at the National Institutes of Health to J.S.N (AR43419). Also, we acknowledge the Institutional support from the Department of Energy, Office of Naval Research, National Institutes of Health and the Beckman Laser Institute and Medical Clinic Endowment. Supported in part (B.M) by Slovenian Ministry of Science and Technology. The experimental work provided by Emil Karapetian and Yung-Hsiang Judy Hsu is also appreciated.

REFERENCES

- [1] Harmon, D.B., 1955, *J. Franklin Inst.* Vol. 259, p.519.
- [2] Tanasawa, Y., and Toyoda, S., 1955, "On the atomization of a liquid jet issuing from a cylindrical nozzle", Tech. Report of Tohoku University N19-2, Japan, p.135.
- [3] Hubbard, G.L., Denny V.E., and Mills, A.F., 1973, "Droplet evaporation: effects of transients and variable properties", *Int. J. Heat and Mass Transfer*, Vol. 16, pp. 1003-1008.
- [4] Kim, Y.M., Kim, S.J., Chen, Z.J., and Chen, C.P., 1998, "Numerical simulation of combustion wave propagation in an air-fuel spray mixture with temperature nonuniformity", *Numerical Heat Transfer Part A-Applications*, Vol. 34, pp. 23-41.
- [5] Ismailov, M.M., Obokata, T., Kobayashi, K., and Polayev, V.M., 1999, "LDA PDA measurements of instantaneous characteristics in high pressure fuel injection and swirl spray", *Experiments In Fluids*, Vol. 27, pp. 1-11.
- [6] Ingebo, R.D., 1991, "Gas property effects on droplet size of simulated fuel sprays", *J. of Propulsion*, Vol. 7, pp. 467-472.
- [7] Ingebo, R.D., 1993, "Effect of vaporization on cryogenic spray droplet size measurement", NASA Technical Memorandum 105909, also in *Proceedings of the 31st Aerospace Sciences Meeting and Exhibit by the AIAA, SAE*, Reno, NV.
- [8] Ingebo, R.D., 1995, "Cryogenic and simulated fuel jet breakup in argon, helium and nitrogen gas flows", NASA Technical Memorandum 106923, also in *Proceedings of the 31st Joint Propulsion Conference cosponsored by the AIAA, SAE, ASME and ASEE*, San Diego, CA.
- [9] Estes, K.A., and Mudawar, I., 1995, "Correlation of Sauter mean diameter and critical heat flux for spray cooling of small surfaces", *International Journal of Heat and Mass Transfer*, Vol. 38, pp. 2985-2996.
- [10] Nelson, J.S., Milner, T.E., Anvari, B., Tanenbaum, B.S., Kimel, S., Svaasand, L.O., and Jacques, S.L., 1995, "Dynamic epidermal cooling during pulsed laser treatment of port wine stain. A new methodology with preliminary clinical evaluation", *Archives of Dermatology*, Vol. 131, pp. 695-700.
- [11] Torres, J.H., Nelson, J.S., Tanenbaum, B.S., Milner, T.E. *et al.*, 1999, "Estimation of internal skin temperatures in response to cryogen spray cooling: Implications for laser therapy of port wine stains", *IEEE Journal of Selected Topics in Quantum Electronics*, Vol. 5, pp. 1058-1066.
- [12] Nelson, J.S., Majaron, B., and Kelly, K.M., to appear in Dec. 2000, "Active skin cooling in conjunction with laser dermatologic surgery: Methodology and clinical results", *Seminars in Cutaneous Medicine and Surgery*.
- [13] Nelson, J.S., Milner, T.E., Anvari, B., Tanenbaum, B.S., *et al.*, 1996, "Dynamic epidermal cooling in conjunction with laser-induced photothermolysis of port wine stain blood vessels", *Lasers in Surgery and Medicine*, Vol. 19, pp. 224-229.
- [14] Chang, C.J., and Nelson, J.S., 1999, "Cryogen spray cooling and higher fluence pulsed dye laser treatment improve port-wine stain clearance while minimizing epidermal damage", *Dermatologic Surgery*, Vol. 25, pp. 767-772.
- [15] Anvari, B., Tanenbaum, B.S., Milner, T.E., Kimel, S., *et al.*, 1995, "A theoretical study of the thermal response of skin to cryogen spray cooling and pulsed laser irradiation - implications for treatment of port wine stain birthmarks", *Physics in Medicine and Biology*, Vol. 40, pp. 1451-1465.
- [16] Verkrusse, W., Majaron, B., Tanenbaum B.S., and Nelson, J.S., in press 2000, "Optimal cryogen spray cooling parameters for pulsed laser treatment of port wine stains", *Lasers in Surgery and Medicine*.
- [17] Aguilar, G., Verkrusse, W., Majaron, B., Zhou, Y., Nelson, J.S., and Lavernia, E.J., 2000, "Modeling cryogenic spray temperature and evaporation rate based on single-droplet, in press", *Proceedings of the Eighth International Conference on Liquid Atomization and Spray Systems*, Pasadena CA, USA.
- [18] Aguilar, G., Majaron, B., Verkrusse, W., Zhou, Y., Nelson, J.S., and Lavernia, E.J., submitted, "Theoretical and experimental analysis of droplet diameter, temperature, and evaporation rate evolution in cryogenic sprays", *Int. J. of Heat and Mass Transfer*.

[19] Verkrusse, W., Majaron, B., Aguilar, G., Nelson, J.S., Svaasand, L.O., 2000, "Dynamics of cryogen deposition in relationship to heat extraction rate during cryogen spray cooling", *Proceedings SPIE*, Vol. 3907, pp. 37-58, San Jose CA.

[20] Svaasand, L.O., Randeberg, L.L., Aguilar, G., Verkrusse, W., Majaron, B., Kimel, S., Nelson, J.S., and Berns, M.W., submitted May 2000, "On the efficacy of cryogen spray cooling during laser induced photothermolysis of port-wine stain vessels", *Physics in Medicine and Biology*.

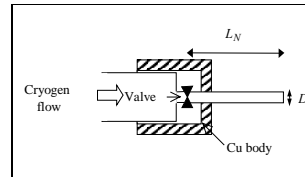
[21] Lefevbre, A.H., *Atomization and Sprays* (1st Edn), p. 309. Taylor & Francis, New York (1989).

[22] Orme, M., 1997, "Experiments on droplet collisions, bounce, coalescence and disruption", *Progress in Energy and Combustion Science*, Vol. 23, pp. 65-79.

[23] Nishitani, R., Kasuya, A., and Nishina, Y., 1993, "Insitu STM observation of coalescence of metal particles in liquid", *Zeitschrift fur Physik D- Atoms, Molecules and Clusters*, Vol. 26, pp. S42-S44.

[24] Li, A., Ahmadi, G., Gaynes, M.A., and Bayer, R.G., 1995, "Aerosol particle deposition in a recirculation region", *Journal of Adhesion*, Vol. 51, pp. 87-103.

[25] Delplanque, J.P., Lavernia, E.J., and Rangel, R.H., 1997, "Numerical investigation of multi-phase flow induced porosity formation in spray-deposited materials", *International Journal of Non-Equilibrium Processing*, Vol. 10, pp. 185-199.



Nozzle	L_N [mm]	D_N [mm]	L_N/D_N
Short wide (SW)	31.8 (1.25 in)	1.4 (0.05 in)	23
Long wide (LW)	63.5 (2.50 in)	1.4 (0.05 in)	46
Short narrow (SN)	31.75 (1.25 in)	0.69 (0.027 in)	46
Long narrow (LN)	63.5 (2.50 in)	0.69 (0.027 in)	93
ScleroPLU S TM	25.4 (1.00 in)	0.76 (0.030 in)	33
GentleLASE TM	18.00 (0.7 in)	0.51 (0.020 in)	35

Table 1. Sketch of straight-tube and Candela nozzle configurations and dimensions.

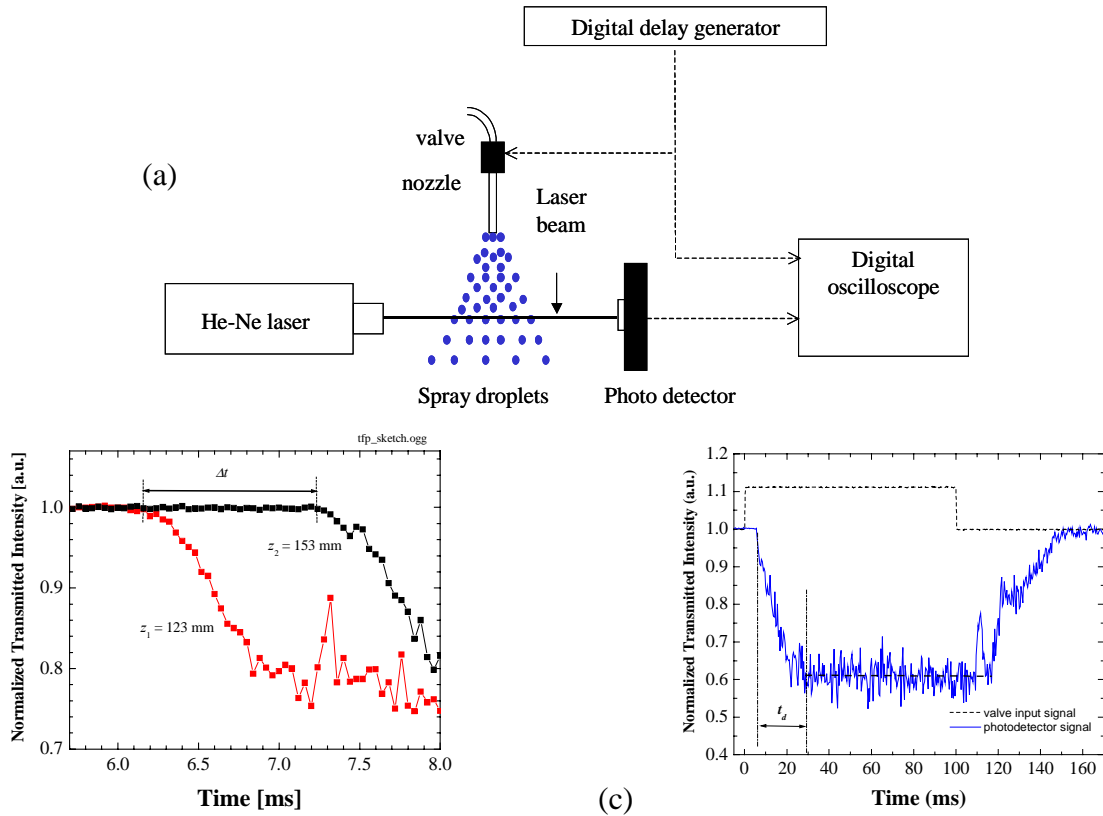


Figure 1: (a) Sketch of time of flight procedure (TFP) setup. (b) Normalized photodetector output signals measured at two distances from the laser beam (123 and 153 mm). The distance between these two locations divided by the time interval between the initiation of the signal attenuation (Δt), equals the average droplet velocity (V). (c) Normalized output signal measured at 60 mm from the nozzle tip for a 100 ms cryogen spurt. The time interval between the valve input signal and that at which the signal reaches a steady state condition is referred to as "spray development time" (t_d).

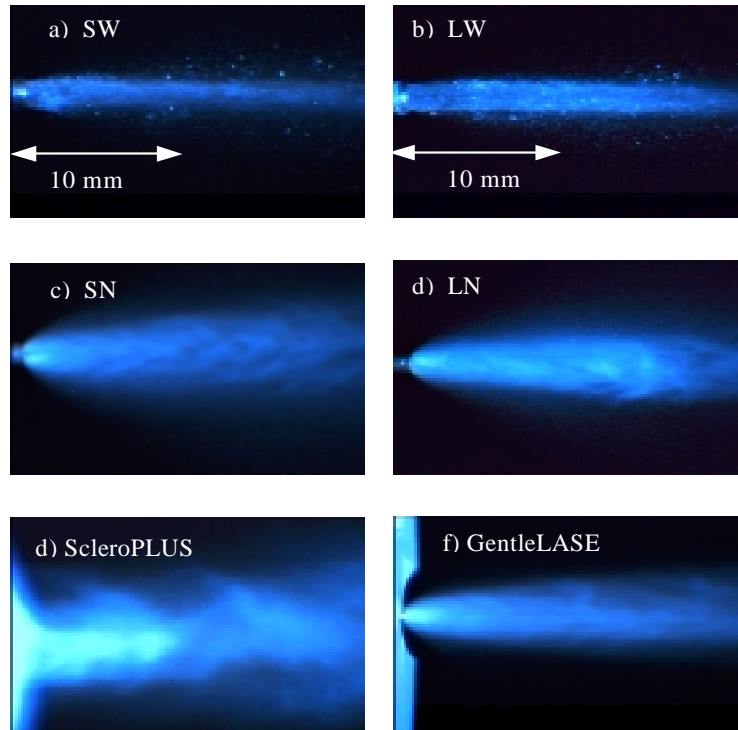


Figure 2. Photographs of cryogenic spray shapes produced by the four straight-tube nozzles and the two Candela nozzles. Length of field of view is 17 mm.

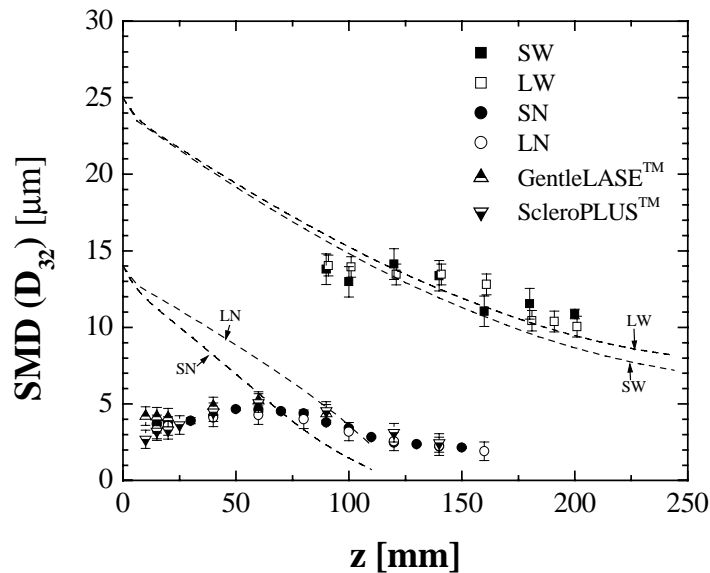


Figure 3. Sauter Mean Diameter (SMD) measurements using the EPCS Insitec/Malvern apparatus. Solid lines represent SMD predicted by the model for the SW and LW nozzles. Dashed lines represent SMD predicted by the model for the SN and LN nozzles. The initial values used in the model for V_0 are: 80, 60, 30 and 15 m/s for SW, LW, SN and LN, respectively; and for D_0 are: 25 and 14 μm for W and N nozzles respectively.

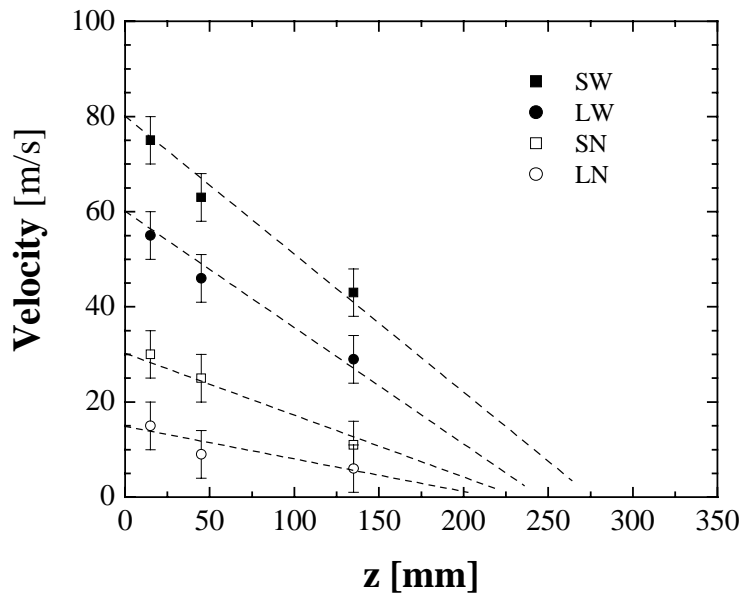


Figure 4. Average droplet velocity evolution with distance from the nozzle tip for the narrow and wide nozzles. Computed using the TFP.

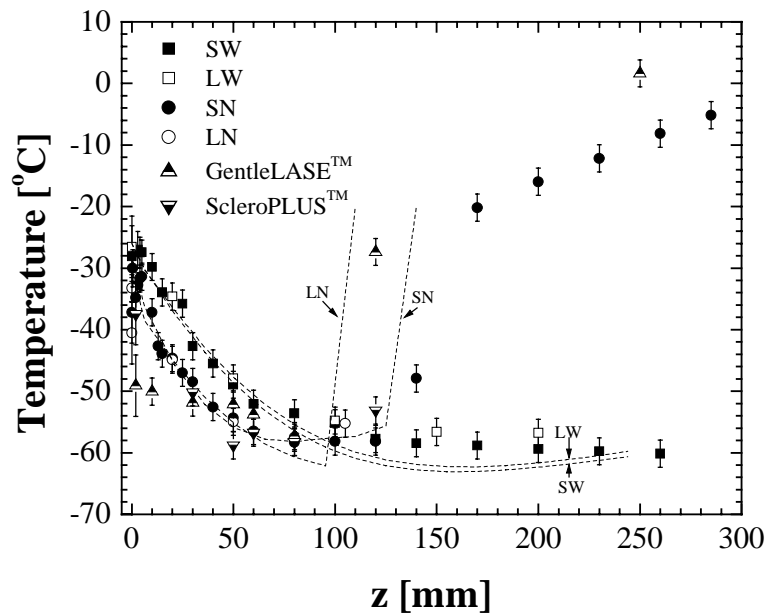


Figure 5. Measurements and model predictions of spray temperatures (T) as a function of distance from the nozzle (z). The initial values used in the model are: $V_{0,SW}=80$ m/s, $V_{0,LW}=60$ m/s, $V_{0,SN}=30$ m/s and $V_{0,LN}=15$ μ m; $D_{0,W}=25$ μ m and $D_{0,N}=14$ μ m; and $T_{0,W}=-26^{\circ}$ C and $T_{0,N}=-29^{\circ}$ C.

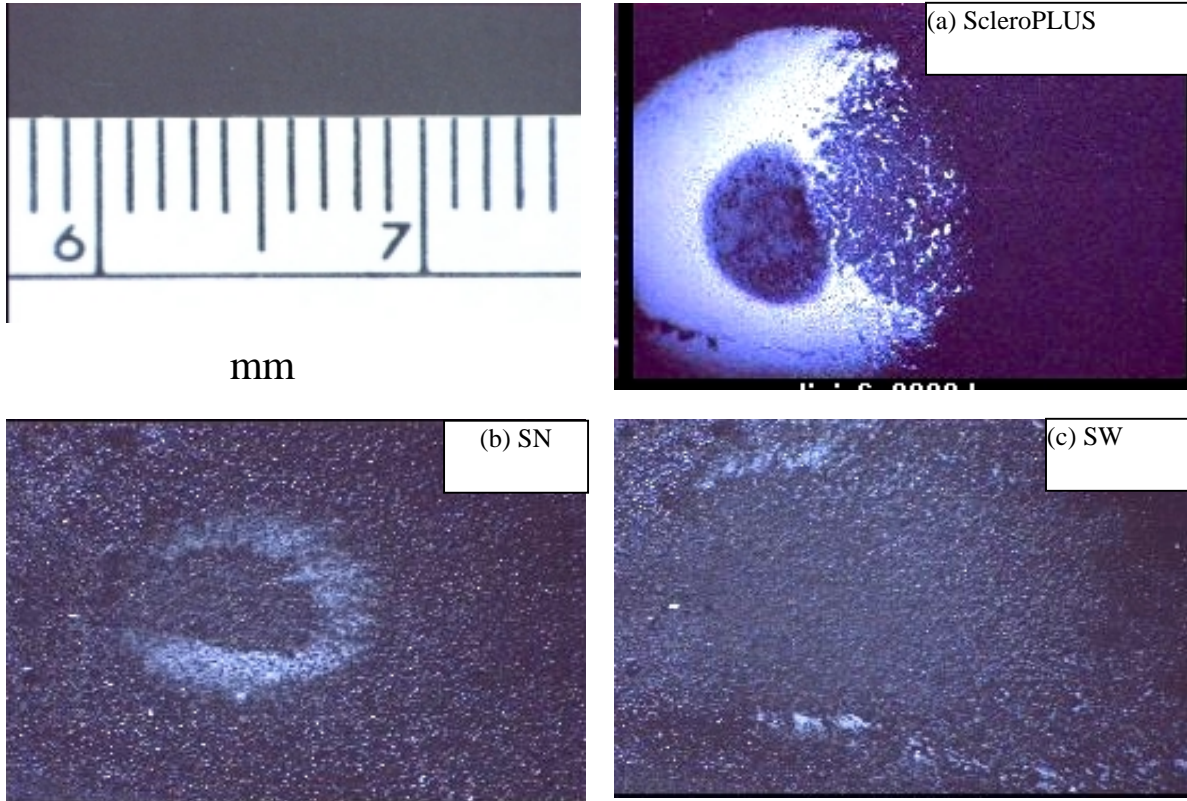


Figure 6. Photographs of frost remaining 2 seconds after the end of 50 ms cryogen spurts on an epoxy block. Nozzles: (A) ScleroPLUSTM, (B) SN, (C) SW. Length of field of view is 17 mm.